MDPI

Article

Safety Analysis, Design and Evaluation of 2-DOF Parallel Lifting Actuator on Stereo Parking Robot

Jingang Jiang *[iD]**, Qiyun Tan, Tianhua He** [iD]**, Jianpeng Sun and Jiawei Zhang**

Key Laboratory of Advanced Manufacturing and Intelligent Technology, Ministry of Education,
Harbin University of Science and Technology, Harbin 150080, China; 2020100037@stu.hrbust.edu.cn (Q.T.);
tianhuah_phd14@hrbust.edu.cn (T.H.); 2110102017@stu.hrbust.edu.cn (J.S.); 2120100044@stu.hrbust.edu.cn (J.Z.)
* Correspondence: jiangjingang@hrbust.edu.cn; Tel.: +86-16608996679; Fax: +86-451-86390485

Abstract: Stereo garage technology can effectively alleviate the problem of parking difficulties, but the safety problems of its actuators, via which the core of stereo parking function can be realized, seriously affect its promotion and further development. In this paper, a two degrees of freedom (2-DOF) parallel lifting actuator for a stereo parking robot is designed by researching the type synthesis of the mechanism based on the screw theory. The limb constrained triangle method, the flexibility of limb constrained triangle, and the failure probability are proposed to determine the final configuration of the parallel lifting actuator. Then, this paper completes the dimensional optimization of the parallel lifting actuator based on the multi-motion performance indexes and kinematic analysis, which improves the safety and stability of the actuator. Finally, this paper verifies the validity of the parallel lifting actuator by establishing a parallel lifting actuator verification model system. By verifying the dynamic characteristics of the model mobile platform under different load conditions, it is proven that the kinematic stability of the mobile platform decreases with the increase of load mass under load conditions. Additionally, through practical application experiment, it is proven that the parallel lifting mechanism can effectively alleviate the parking difficulty problem.

Keywords: parallel lifting actuator; stereo parking robot; type synthesis; kinematic analysis; safety and stability

1. Introduction

With the rapid development of the economy, the number of cars in China reached 281 million by the end of 2020, which has also brought significant challenges to the parking industry [1,2]. At present, the parking problem has become a common problem in daily life, and sometimes even seriously affects people's lives. The emergence of stereo parking equipment has effectively alleviated the current parking difficulties and facilitated people's daily life [3,4]. Therefore, in recent years, many scholars have carried out extensive research on stereo parking equipment to better solve the parking difficulty problem. In stereo parking equipment, the lifting actuator of the stereo parking equipment is the core actuator for the realization of the stereo parking function. For this reason, the research on the stereo parking actuator has become one of the hot spots for research and has become the key to solving the parking problem.

Among them, Song Qiuhong et al. [5] proposed a push–pull driving actuator of a tree-like stereo garage and verified the feasibility and stability of the actuator, which provided a great help for the optimization design of the automatic push–pull drive actuator in the later stage. Zheng Rui et al. [6] designed an actuator for oblique stereo parking equipment using the crank linkage mechanism, which improved the space utilization and reduced the manufacturing and operating costs. Zhang Wenjie et al. [7] proposed a new design scheme for the actuator of the stereo parking device. The actuator in this scheme is driven by connecting rods, gears, and racks, which is universal and can be applied in public

areas. Wang Zhongyuan et al. [8] proposed a four-bar actuator based on the ADAMS for application to non-avoidance side direction stereo parking equipment, which improves the rationality of the four-bar lifting mechanism and reduces the cost of the equipment. Yang Jianqiang et al. [9] designed an actuator using chains, sprockets, pulleys and tracks for transmission, which is able to realize the integration of movement (or rotation) and lifting, further improving the efficiency. Xia Qi et al. [10] designed a new type of comprehensive parking device, which uses the double crank actuator and lifting actuator to realize the function of parking six cars in two parking spaces. Ye Jiagen et al. [11] designed a stereo parking actuator driven by connecting rods and guide rails based on the consideration of parking space and parking method, which can work automatically with the advantages of simple operation and time saving. Zhang Liping et al. [12] designed a multi-service station parking equipment for hydraulic clip lifting and reversing. The actuator of this equipment is driven by the chains and sprockets, which can realize multi-service processing and effectively improve the efficiency of vehicle access. Wang Yuehong [13] proposed a simple stereo parking equipment based on the requirement of a no-avoidance relationship and equipment stability. The mechanism is composed of the planetary gear actuator and parallelogram actuator, and is driven by chains and gears. Zhang Tianyu et al. [14] designed a small stereo parking actuator consisting of the stereo frame, the vertical lifting mechanism, the horizontal rotary platform, the movable parking space and the transmission system. This actuator can realize the lifting and docking of movable parking spaces to store and extract vehicles. Chen Zhihua et al. [15] proposed a novel gait transition hierarchical control framework for the developed hexapod wheel-legged robot, and the experimental results show that the robot can modify the foot-end trajectory in dynamic unstructured terrain and obtain elastic gait in obstacle avoidance. The above researchers have performed a useful exploration of the stereo parking actuator, but these stereo parking actuators are usually steel structure frames. As most of them use chains, gears, connecting rods, and other mechanisms for transmission, such structures are prone to cause equipment failure due to the failure of the frame and transmission components and the long transmission chain, and, thus, to cause serious accidents, bringing property damage and personal injury, and reducing people's trust in the stereo garage. This greatly affects the application and popularity of stereo parking technology, and the problem of difficult parking cannot be effectively solved by stereo parking technology.

To address the above problems, this paper proposed a 2-DOF parallel lifting actuator on a stereo parking robot by analyzing the form, size, and functional requirements of the stereo garage. In addition, the specific contributions of this paper are as follows: (1) according to the advantages of the parallel mechanism, such as high rigidity, short transmission chain, stable structure, and low motion inertia [16], the parallel mechanism is introduced into the stereo parking robot, and a comprehensive research of the type synthesis is carried out based on the screw theory; (2) the limb constrained triangle method is proposed to solve the problem that the movement DOF along *Y*-axis of the parallel actuators cannot be constrained; (3) in order to make the modified mechanism have the same motion properties as the original mechanism as far as possible, the flexibility of limb constraint triangle is proposed; (4) the configuration of the parallel lifting actuator is finally determined by combining the proposed method of selecting the driving link based on the failure probability and the results of the comparative analysis of the parallel mechanism by ADAMS; (5) the dimensional optimization of the actuator is completed through kinematic analysis and multi-motion performance indexes, which further improves the safety and stability of the actuator; (6) by constructing the verification model system and the practical application experiment, it is proven that the actuator can effectively solve the safety and stability problems of the stereo parking equipment, promote the development and further popularization of the stereo parking technology, and more effectively alleviate the problem of parking difficulties. The framework of this paper is shown in Figure 1.
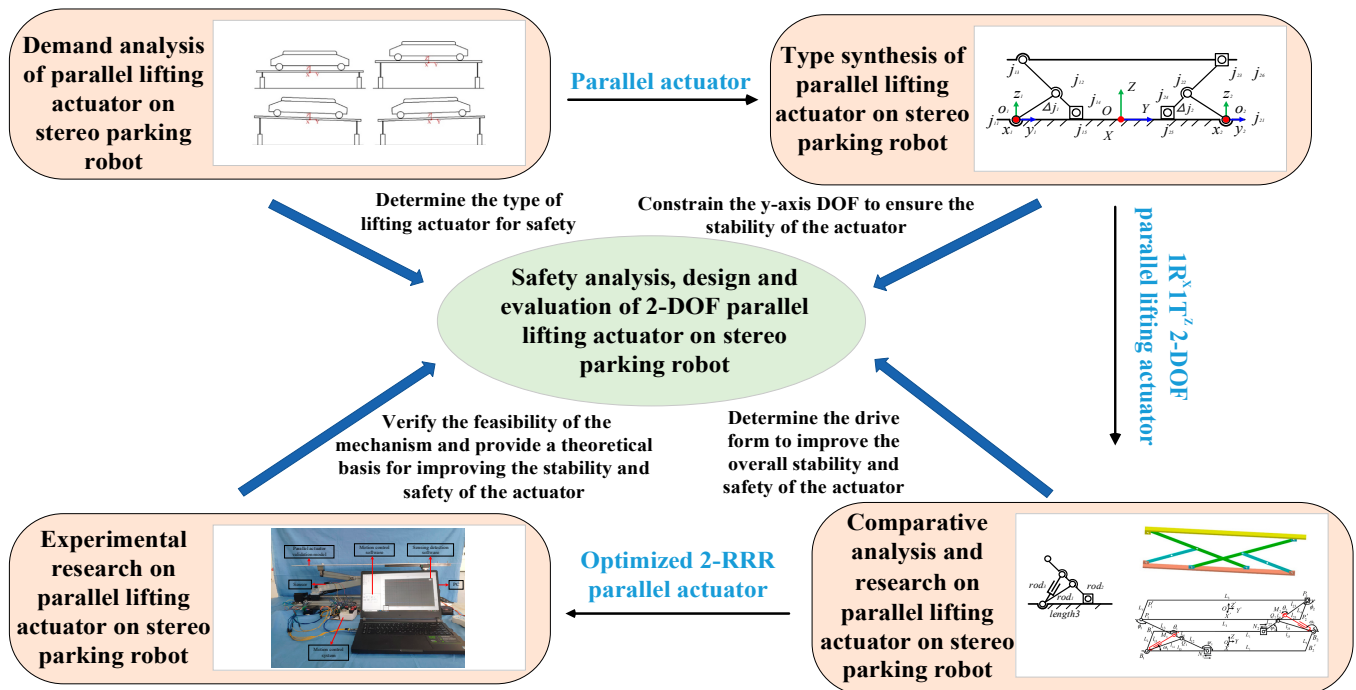
Figure 1. The proposed framework for a 2-DOF parallel lifting actuator on a stereo parking robot.

2. Type Synthesis Research of Parallel Lifting Actuator on Stereo Parking Robot

2.1. Demand Analysis of Parallel Lifting Actuator on Stereo Parking Robot

Through the analysis of the simple elevator type equipment, lifting-transferring type equipment, and a special parking robot, it can be concluded that a stereo garage using pallet-type equipment can use the multi-floor space more effectively and are less prone to generate vibration and stress concentration during the process of lifting the vehicle. Therefore, the lifting actuator of stereo parking robot was proposed to use the form of parallel pallet lifting, and the required DOFs are the movement DOF along the *Z*-axis and the rotation DOF around the *X*-axis. The rotation DOF is set to deal with structural problems, such as the adverse vibration caused by the offset of the vehicle barycenter and the failure of the kinematic chain to ensure safety and stability. Therefore, the parallel lifting actuator required by the stereo parking robot can be determined as a $1R^X1T^Z$ 2-DOF parallel actuator. The blueprint of the parallel lifting actuator applied on a stereo parking robot is shown in Figure 2.
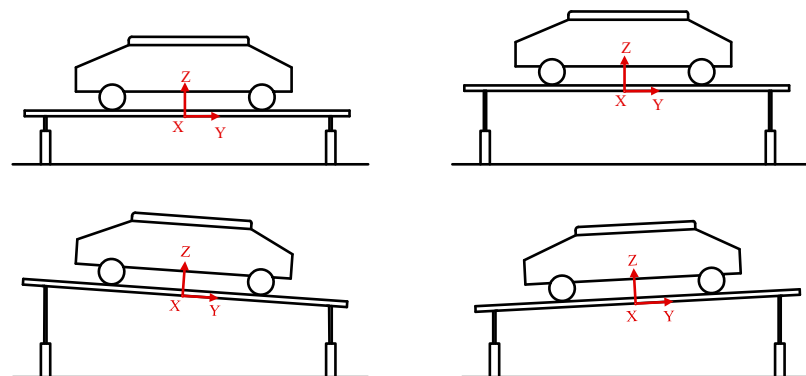
Figure 2. Blueprint of a parallel lifting mechanism applied on a stereo parking robot.

2.2. Analysis of Constraint Screw System of 2-DOF Parallel Actuator

The screw theory is widely used in academia for the analysis of mechanisms, mechanism kinematics, and dynamics. By using the screw method to analyze the kinematic screw

and constraint screw of the $1R^X1T^Z$ 2-DOF parallel actuator, the desired configuration of the parallel actuator can be synthesized.

The $1R^X1T^Z$ 2-DOF parallel actuator has one rotation DOF around the *X*-axis and one movement DOF along the *Z*-axis, and its basic kinematic screw is expressed as follows:

$$\begin{aligned} S_1 &= (\ 1\quad 0\quad 0\quad ;\quad 0\quad 0\quad 0\ )\\ S_2 &= (\ 0\quad 0\quad 0\quad ;\quad 0\quad 0\quad 1\ )\end{aligned} \tag{1}$$

The basic constraint screw can be obtained by calculating the inverse screw of the basic kinematic screw, as follows:

$$\begin{aligned} S_1^r &= (\ 1\quad 0\quad 0\quad ;\quad 0\quad 0\quad 0\ )\\ S_2^r &= (\ 0\quad 1\quad 0\quad ;\quad 0\quad 0\quad 0\ )\\ S_3^r &= (\ 0\quad 0\quad 0\quad ;\quad 0\quad 1\quad 0\ )\\ S_4^r &= (\ 0\quad 0\quad 0\quad ;\quad 0\quad 0\quad 1\ )\end{aligned} \tag{2}$$

where S_1^r and S_2^r represent the constraint force screws along the *X*-axis and *Y*-axis, respectively, while S_3^r and S_4^r represent the constraint couples along the *Y*-axis and *Z*-axis, respectively. The $1R^X1T^Z$ 2-DOF parallel actuator is constrained with four DOFs in cartesian space, and the basic constraint screw system contains four constraint screws, which is called the constraint-4 screw system. Since the kinematic screws are constrained by the constraint couple, the constraint force line vector and constraint force screw in space are different due to the difference in the number, combination, and geometric relationship of the constraint couple, constraint force line vector, and constraint force screw, the analysis of the constraint screw system of the common 2-DOF actuator is required to form the above constraints. Generally, due to the complexity of the screw pair and the constraint force screw in space, the screw pair is not used in the parallel actuator. Therefore, only the constraint couple and the constraint force line vector are considered in the analysis of the constraint screw system of the parallel actuator.

2.3. Research on the Constraint-4 Screw System Based on the Fixed-Rotation Screw System Method

In the common constraint screw system, each constraint couple and constraint force line vector are independent of each other. Therefore, there are three cases in the composition of the constraint-4 screw system, as follows: the constraint screw system A is composed of three constraint couples and one constraint force line vector; the constraint screw system B is composed of two constraint couples and two constraint force line vectors; the constraint screw system C is composed of one constraint couple and three constraint force line vectors.

In this section, an analysis method of the constraint-4 screw system, called the fixed-rotation screw system method, is proposed based on the fact that the constraint couple is the free vector, and that the constraint force line vector is the line vector in space. In this method, a fixed constraint screw system and a rotation constraint screw system are set up in space, and the constraint force line vector and the constraint couple are placed in the fixed constraint screw system and the rotation constraint screw system, respectively. The origin of the fixed constraint screw system coincides with the origin of the world coordinate system, and the coordinate axes of the fixed constraint screw system coincide with the coordinate axes of the world coordinate system, respectively, and can only be rotated about the world coordinate system, while the rotation constraint screw system is in a free state in the cartesian coordinate system, and can be both rotated about the world coordinate system and moved relative to the world coordinate system.

According to this method, the constraint-4 screw systems are analyzed, and there are two types of constraint screw systems that can satisfy the DOF requirements of the 2-DOF parallel lifting actuator, as shown in Table 1.

The rigid body has a movement DOF along the *Z*-axis and a rotation DOF around the *Z*-axis under the action of the basic constraint screw system S_a^r. When the rotation constraint

screw system rotates $\frac{\pi}{2}$ around the *Y*-axis, S^r_{3a} becomes $S''^r_{3a} = \begin{pmatrix} 0 & 0 & 0 & ; & 0 & 0 & 1 \end{pmatrix}$, which constrains the rotation DOF around the *Z*-axis, and the rigid body has a rotation DOF around the *X*-axis and a movement DOF along the *Z*-axis, which meets the DOF requirements of the 2-DOF parallel lifting actuator on the stereo parking robot.

Table 1. Two constraint screw systems meet the requirements.

Constraint Screw System B	Constraint Screw System C
a. The couples are coplanar and intersectant, the force line vectors are coplanar and intersectant	b. The force line vectors are coplanar and disjoint, the couple parallels to the coordinate axis
Basic constraint screw system S^r_a	Basic constraint screw system S^r_b
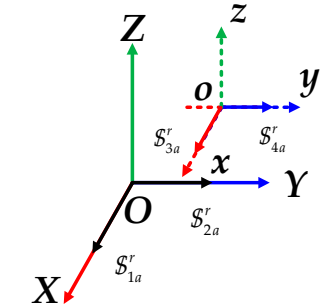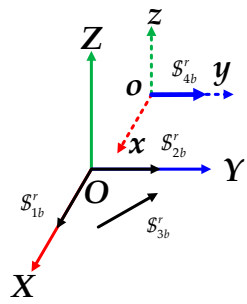
The three coplanar and disjoint constraint force line vectors constrain all movement DOFs along the two axes in the plane where they are located, and also constrain the rotation DOF around the axis which are perpendicular to the plane where they are located. The rigid body has two rotation DOFs when the axis of the only constraint couple is perpendicular to the plane where the constraint force line vectors are located, and, conversely, the rigid body has one rotation DOF. At this point, the rigid body has one rotation DOF around the *X*-axis and one movement DOF along the *Z*-axis under the action of the constraint screw system S^r_b, which meets the DOF requirements the of 2-DOF parallel lifting actuator on the stereo parking robot.

2.4. Type Synthesis Analysis of $1R^X1T^Z$ 2-DOF Parallel Actuator Based on the Limb Constrained Triangle

According to the analysis in the previous section, there are two types of constraint screw systems that can satisfy the DOF requirements of the 2-DOF parallel lifting actuator, which are S''^r_a and S^r_b. By analyzing the S''^r_a and S^r_b, we can determine the following:

$$S''^r_a = \begin{pmatrix} S^r_{1a} = \begin{pmatrix} 1 & 0 & 0 & ; & 0 & 0 & 0 \end{pmatrix} \\ S^r_{2a} = \begin{pmatrix} 0 & 1 & 0 & ; & 0 & 0 & 0 \end{pmatrix} \\ S''^r_{3a} = \begin{pmatrix} 0 & 0 & 0 & ; & 0 & 0 & 1 \end{pmatrix} \\ S^r_{4a} = \begin{pmatrix} 0 & 0 & 0 & ; & 0 & 1 & 0 \end{pmatrix} \end{pmatrix} \tag{3}$$

Obviously, if the constraint screw system provided by a limb kinematic chain is exactly same as S''^r_a, then the basic kinematic screws of the series limb are $\begin{pmatrix} 1 & 0 & 0 & ; & 0 & 0 & 0 \end{pmatrix}$ and $\begin{pmatrix} 0 & 0 & 0 & ; & 0 & 0 & 1 \end{pmatrix}$, and the linear combination of these two basic kinematic screws is not able to form a valid limb kinematic chain in space. Therefore, according to the different types and quantities of constraint screws of the limb kinematic chain in S''^r_a, it can be divided into three cases, as shown in Table 2.

As shown in Table 2, on the basis of the obtained kinematic screws of the limb kinematic chain (hereinafter referred to as limb kinematic screws), the limb kinematic screws can be linearly combined to obtain a new limb kinematic screw, and the appropriate limb kinematic chains will be obtained by the reasonable combination of the above kinematic screws.

Table 2. Constraint screw of limb kinematic chain S''^r_a.

A. Constraint Force Line Vector × 2 Constraint Couple × 1	B. Constraint Force Line Vector × 1 Constraint Couple × 2	C. Constraint Force Line Vector × 1 Constraint Couple × 1
Constraint screws of limb kinematic chain		
$S''^{r1}_a = (\ 1\quad 0\quad 0\ ;\ 0\quad 0\quad 0\ )$ $S''^{r2}_a = (\ 0\quad 1\quad 0\ ;\ 0\quad 0\quad 0\ )$ $S''^{r3}_a = (\ 0\quad 0\quad 0\ ;\ 0\quad 1\quad 0\ )$	$S''^{r4}_a = (\ 1\quad 0\quad 0\ ;\ 0\quad 0\quad 0\ )$ $S''^{r5}_a = (\ 0\quad 0\quad 0\ ;\ 0\quad 1\quad 0\ )$ $S''^{r6}_a = (\ 0\quad 0\quad 0\ ;\ 0\quad 0\quad 1\ )$	$S''^{r7}_a = (\ 1\quad 0\quad 0\ ;\ 0\quad 0\quad 0\ )$ $S''^{r8}_a = (\ 0\quad 0\quad 0\ ;\ 0\quad m_{d8}\quad n_{d8}\ )$
Geometric relationship between the constraint screws of limb kinematic chain		
The force line vectors are coplanar and parallel, the couples are parallel	The force line vectors are coplanar and intersectant, the couples are parallel	The force line vectors are coplanar and intersectant, the couples are parallel
Basic constraint screws of limb kinematic chain		
$S'^1_a = (\ 1\quad 0\quad 0\ ;\ 0\quad 0\quad 0\ )$ $S'^2_a = (\ 0\quad 0\quad 1\ ;\ 0\quad 0\quad 0\ )$ $S'^3_a = (\ 0\quad 0\quad 0\ ;\ 0\quad 0\quad 1\ )$	$S'^4_a = (\ 1\quad 0\quad 0\ ;\ 0\quad 0\quad 0\ )$ $S'^5_a = (\ 0\quad 0\quad 0\ ;\ 0\quad 1\quad 0\ )$ $S'^6_a = (\ 0\quad 0\quad 0\ ;\ 0\quad 0\quad 1\ )$	$S'^7_a = (\ 1\quad 0\quad 0\ ;\ 0\quad 0\quad 0\ )$ $S'^8_a = (\ 0\quad n_{a8}\quad m_{a8}\ ;\ 0\quad 0\quad 0\ )$ $S'^9_a = (\ 0\quad 0\quad 0\ ;\ 0\quad 1\quad 0\ )$ $S'^{10}_a = (\ 0\quad 0\quad 0\ ;\ 0\quad 0\quad 1\ )$
Kinematic screws of the new limb kinematic chain obtained by linear combination		
$S'^1_{an} = (\ l_{an1}\quad 0\quad n_{an1}\ ;\ 0\quad 0\quad 0\ )$ $S'^2_{an} = (\ 1\quad 0\quad 0\ ;\ 0\quad 0\quad r_{an2}\ )$	$S'^3_{an} = (\ 1\quad 0\quad 0\ ;\ 0\quad q_{an3}\quad 0\ )$ $S'^4_{an} = (\ 1\quad 0\quad 0\ ;\ 0\quad 0\quad r_{an3}\ )$ $S'^5_{an} = (\ 1\quad 0\quad 0\ ;\ 0\quad q_{an4}\quad r_{an4}\ )$ $S'^6_{an} = (\ 0\quad 0\quad 0\ ;\ 0\quad m_{an5}\quad n_{an5}\ )$	$S'^7_{an} = (\ 1\quad 0\quad 0\ ;\ 0\quad q_{an7}\quad 0\ )$ $S'^8_{an} = (\ 1\quad 0\quad 0\ ;\ 0\quad 0\quad r_{an8}\ )$ $S'^9_{an} = (\ 1\quad 0\quad 0\ ;\ 0\quad q_{an9}\quad r_{an9}\ )$ $S'^{10}_{an} = (\ 0\quad 0\quad 0\ ;\ 0\quad m_{an10}\quad n_{an10}\ )$ $S'^{11}_{an} = (\ l_{an11}\quad m_{an11}\quad n_{an11}\ ;\ 0\quad 0\quad 0\ )$

Among them, the limb kinematic chain of type A contains three constraint screws, and the corresponding limb kinematic chain has three DOFs. There are five kinds of kinematic screws that can be used to construct the limb kinematic chain, where S'^1_{an} represents the couple screw whose axis of rotation is located in the XOZ plane, S'^2_{an} represents the couple screw whose axis is located in the XOY plane. The direction is parallel to the *X*-axis. These couples and line vectors can only form the instantaneous limb kinematic chain.

The limb kinematic chain of type B contains three constraint screws, the corresponding limb kinematic chain has three DOFs, and the kinematic screw contains three force line vector screws and four couple screws. The force line vector screws represent the prismatic pair along *Y*-axis, the prismatic pair along *Z*-axis and the prismatic pair whose axis is located in the YOZ plane, respectively, and the rotation axes of the couple screws are parallel to the *X*-axis. When the force line vectors are combined with the couples, the prismatic pairs along the *Y*-axis and the *Z*-axis are called the instantaneous prismatic pair, and the prismatic pair whose axis is located in the YOZ plane is not affected. Therefore, the S'^4_a, S'^5_{an}, and S'^5_{an} can form the first limb kinematic chain, and the S'^4_a, S'^6_{an}, and S'^5_{an} can form the second limb kinematic chain.

The limb kinematic chain of type C contains two constraint screws, the corresponding limb kinematic chain has four DOFs, and the kinematic screw contains five couple screws, three force line vector screws, and one helical screw. Furthermore, S'^7_{an} represents the rotation pair located in the XOZ plane with the axis parallel to the *X*-axis, S'^8_a represents the rotation pair whose axis is located in the YOZ plane, S'^9_{an} represents the rotation pair located at any position in space with the axis parallel to the *X*-axis, S'^{10}_{an} represents the prismatic pair whose axis is located in the YOZ plane, and S'^{11}_{an} represents a ball pair. Since the helical pair is complicated and cumbersome in practical application, the appearance of the helical pair will be avoided in the type synthesis process of the actuator. Therefore, in the basic screw, S'^8_a can only be linearly combined with S'^7_a.

The reasonable combination of the limb kinematic chain screws are S'^4_a-S'^5_{an}-S'^5_{an} and S'^4_a-S'^6_{an}-S'^5_{an}, as shown in Figure 3.
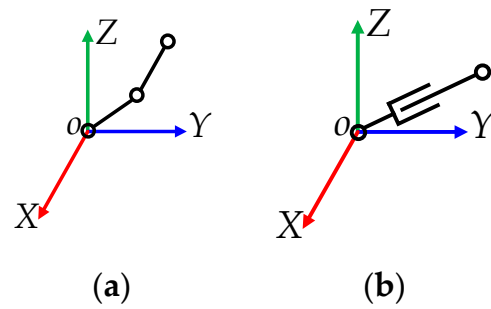
Figure 3. Screws combination of the limb kinematic chain: (**a**) S'^4_a-S'^5_{an}-S'^5_{an} (RRR); (**b**) S'^4_a-S'^6_{an}-S'^5_{an} (RPR).

The two limb kinematic chains are symmetrically arranged between the fixed platform and the mobile platform, as shown in Figure 4. By calculating the DOF of two actuators, it can be obtained that the two types of parallel actuators have three DOFs and require three driving links. The three DOFs are the movement DOF along the Y-axis, the movement DOF along the Z-axis, and the rotation DOF around the X-axis. Compared with the two DOFs of $1R^X1T^Z$, the movement DOF along the Y-axis of the above two types of parallel actuators are not restricted. Reference [17] shows that in order to ensure the constraint force line vectors are coplanar and intersectant and the constraint screws are parallel, the form and layout of the limb kinematic chains in the actuator need to meet the following conditions: the center points of each limb kinematic chain are coincident, then the constraint force line vectors can be coplanar and intersectant; in each limb kinematic chain, the axes between the rotation pairs with parallel axes must be kept parallel at all times, and cannot be an instantaneous mechanism.
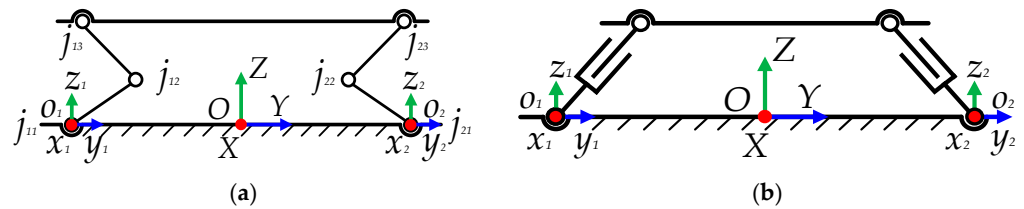
Figure 4. Symmetrical arrangement of two kinds of limb kinematic chains: (**a**) Symmetrical arrangement of the RRR limb kinematic chain; (**b**) Symmetrical arrangement of the RPR limb kinematic chain.

The limb center point of the actuator is the intersection point of the rotation pairs that are not parallel to any coordinate axis in the limb kinematic chain. Combined with the fixed-rotation screw system method, the limb center point can be interpreted as the origin of the fixed-rotation screw system. During the motion of the limb kinematic chain, the origin of the fixed-rotation screw system also changes in real time. Since the constraint force line vectors are not free vectors, if the constraint force line vectors in different limb kinematic chains are coplanar and intersectant under the case that the constraint screws of each branch kinematic chain are exactly the same, only the origins of the fixed-rotation screw systems are coincident. Since the constraint couples are free vectors, if the constraint couples are to be parallel, only the coordinate axes of the fixed-rotation screw systems need to be parallel to each other.

In the two limb kinematic chains of RRR and RPR, there is no intersection point of each limb fixed-rotation screw systems, so there is no constraint on movement DOF along the Y-axis. Due to the need to avoid actuation redundancy and meet the requirement of symmetrical arrangement of limb kinematic chains, the fixed-rotation screw systems of each limb kinematic chain cannot form an angle, so the constraint force line vectors cannot be coplanar and intersectant.

The RRR limb kinematic chain and the RPR limb kinematic chain are modified without changing the limb DOF.

Taking the RRR limb kinematic chain as an example, the connecting rod between the rotation pairs j_2 and j_3 are extended, respectively, and connected with the frame by the rotation pair (same kinematic screw as S'^4_{an}) and the prismatic pair (same kinematic screw as S'^5_a) to form a limb constrained triangle Δj, as shown in Figure 5a.

(**a**)　　　　　　　　　　　　　　　　(**b**)
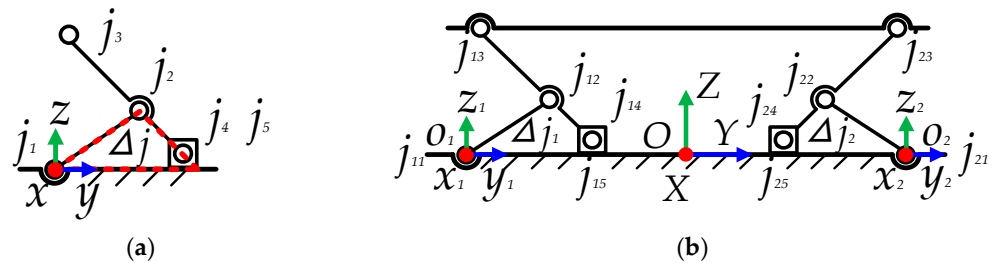
Figure 5. Parallel platform constructed by the RRR limb kinematic chain with a constrained triangle: (**a**) RRR limb kinematic chain with a constrained triangle; (**b**) Mobile platform.

For the limb kinematic chain shown in Figure 5a, the kinematic screws of the five kinematic pairs are as follows:

$$
\begin{aligned}
j_1 &= (\ 1 \quad 0 \quad 0 \quad ; \quad 0 \quad 0 \quad 0\ ) \\
j_2 &= (\ 1 \quad 0 \quad 0 \quad ; \quad 0 \quad q_{j_2} \quad r_{j_2}\ ) \\
j_3 &= (\ 1 \quad 0 \quad 0 \quad ; \quad 0 \quad q_{j_3} \quad r_{j_3}\ ) \\
j_4 &= (\ 1 \quad 0 \quad 0 \quad ; \quad 0 \quad 0 \quad r_{j_4}\ ) \\
j_5 &= (\ 0 \quad 0 \quad 0 \quad ; \quad 0 \quad 1 \quad 0\ )
\end{aligned}
\tag{4}
$$

The inverse screws of the above kinematic screws can be obtained as follows:

$$
\begin{aligned}
j_1^r &= (\ 0 \quad 0 \quad 0 \quad ; \quad 0 \quad 1 \quad 0\ ) \\
j_2^r &= (\ 0 \quad 0 \quad 0 \quad ; \quad 0 \quad 0 \quad 1\ ) \\
j_3^r &= (\ 1 \quad 0 \quad 0 \quad ; \quad 0 \quad 0 \quad 0\ )
\end{aligned}
\tag{5}
$$

The above kinematic screws can be obtained by the linear combination of the basic kinematic screw of the B type limb kinematic chain, and the inverse screws are the same as the constraint screw of the B type limb kinematic chain, so the limb constrained triangle does not affect the original DOF of the limb kinematic chain. However, due to the existence of the limb constrained triangle, the movement DOF of the limb kinematic chain in the YOZ plane are limited.

The real unit of the kinematic screw of the rotation pair represents the direction cosine of the rotation axis, and the dual unit is the component of the moment of the rotation axis to the origin on each axis. Since the rotation axes of j_1, j_2, j_3, and j_4 are parallel to the X-axis, each component of the dual unit can also be used to represent the distance from the origin to the axis. In $\Delta x j_2 j_4$, the lengths of each side are as follows:

$$
\begin{aligned}
l_{j_2 j_4} &= \sqrt{q_{j_2}^2 + (r_{j2} - r_{j4})^2} \\
l_{x j_4} &= r_{j_4} \\
l_{x j_2} &= \sqrt{q_{j_2}^2 + r_{j_2}^2}
\end{aligned}
\tag{6}
$$

According to the law of the trilateral relationship of the triangle, $l_{x j_2}$ and $l_{j_2 j_4}$ are both fixed values, thus, the length of the three sides must satisfy $l_{x j_2} + l_{j_2 j_4} > l_{x j_4}$, and Formula (7) can be obtained as follows:

$$
r_{j_4}^2 - 4 r_{j_4} q_{j_2} < 4 r_{j_2}^2
\tag{7}
$$

Although the number and the properties of the DOF contained in the limb kinematic chain have not changed, its movement in the YOZ plane still needs to meet the condition of

Formula (7). When the two sets of limb kinematic chains are symmetrically arranged, the rotation DOF of the actuator around the *X*-axis is constrained. Meanwhile, as shown in Figure 5b, the movement DOF of the actuator along the *Y*-axis is also limited under the joint constraint of the limb constrained triangles Δj_1 and Δj_2, as well as the fixed-length mobile platform $j_{13}j_{23}$. Including the frame, the reconstructed RRR limb kinematic chain parallel actuator contains eight components, eight rotation pairs and two prismatic pairs, and there is no redundant constraint. The actuator has only one DOF and one driving link, and the DOF of the actuator is the movement DOF along the *X*-axis.

Based on the above analysis, in order to obtain the rotation DOF of the actuator, it is only necessary to constrain the constraint force line vectors within the constraint range of the constrained triangle to be non-parallel. The actuator shown in Figure 5b is modified. As shown in Figure 6, a prismatic pair j_{26} is added to the rotation pair of j_{23}, and its kinematic screw is $j_{26} = \begin{pmatrix} 0 & 0 & 0 & ; & 0 & m_{j_{26}} & n_{j_{26}} \end{pmatrix}$, which does not change the DOF and property of the limb kinematic chain.
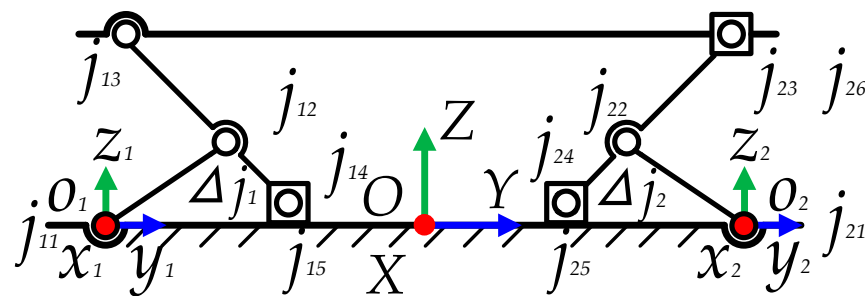
Figure 6. Parallel platform constructed by the RRR limb kinematic chain with a modified constrained triangle.

Including the frame, this actuator contains nine components, eight rotation pairs and three prismatic pairs. There is no redundant constraint, and the modified actuator has two DOFs and requires two driving links. After the modification, the direction of the constraint force line vectors within the range of two limb constrained triangles can be changed, and the distance between $j_{13}j_{23}$ can also be changed.

Based on the above analysis, as shown in Figure 7, the rotation center point of the parallel actuator is time-varying and does not coincide with the coordinate origin.
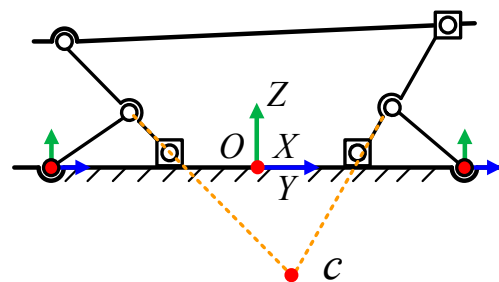
Figure 7. Position and posture of the RRR limb kinematic chain parallel platform.

Similarly, the $1R^X1T^Z$ parallel actuator composed of the RPR series limb is shown in Figure 8. Including the frame, this actuator contains nine components, eight rotation pairs, three prismatic pairs, two driving links are required, and there is no redundant constraint. The DOF number of the RPR limb parallel actuator modified by the constrained triangle method is two, which are the movement DOF along the *Z*-axis and the rotation DOF around the *X*-axis, which meets the DOF requirements of the $1R^X1T^Z$ parallel actuator.
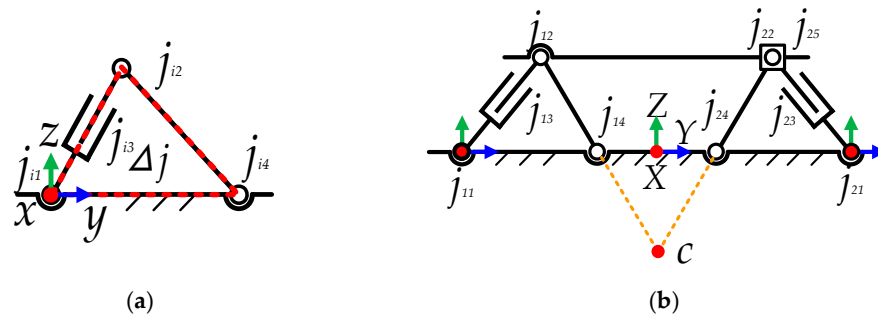
Figure 8. Parallel platform constructed by the RPR limb kinematic chain with a modified constrained triangle: (**a**) Parallel platform constructed by the RPR limb kinematic chain with a modified constrained triangle; (**b**) Mobile platform.

3. Comparison Analysis of the Parallel Lifting Actuator on Stereo Parking Robot

3.1. Comparison Analysis of Configurations Based on the Flexibility of Limb Constrained Triangle

In the two parallel actuators, the starting points of the limb constrained triangle are the j_{23} ($i = 1, 2$) joint of the respective limb kinematic chain. When the motion of the limb kinematic chain is restricted by the limb constrained triangle, the extent of restriction of the limb kinematic chain can be known by analyzing and researching the motion range of the j_{i2} joint.

Given the length of the fixed-length rods in the two limb kinematic chains, as shown in Table 3, the lengths of the fixed-length rods in two limb kinematic chains are equal.

Table 3. Parameters of two kinds of limb kinematic chain.

The Length of Each Part of the RRR Limb Kinematic Chain (mm)			The Length of Each Part of the RPR Limb Kinematic Chain (mm)		
$l_{j_{i1}j_{i2}}$	$l_{j_{i2}j_{i4}}$	$l_{j_{i1}j_{i4}}$	$l_{j_{i1}j_{i2}}$	$l_{j_{i2}j_{i4}}$	$l_{j_{i1}j_{i4}}$
1750	1750	variable	variable	1750	1750

In the RRR limb kinematic chain, the position of joint j_{i2} is as follows:

$$y_{Rj_{i2}} = \frac{l_{xj_{i4}}}{2}, z_{Rj_{i2}} = \sqrt{l^2_{j_{i1}j_{i2}} - \left(\frac{l_{xj_{i4}}}{2}\right)^2} \tag{8}$$

In the RPR limb kinematic chain, the position of joint j_{i2} is as follows:

$$\cos j_{i1} = \frac{l^2_{xj_{i2}}}{2l_{xj_{i2}}l_{xj_{i4}}}, y_{Pj_{i2}} = l_{xj_{i2}} \cos j_{i1}, z_{Pj_{i2}} = \sqrt{l^2_{xj_{i2}} - y^2_{Pj_{i2}}} \tag{9}$$

As described in Section 2.4, the constraint force screw will not satisfy the movement limit that the sum of the length of the fixed side is greater than the length of the variable length side of the limb constrained triangle. According to the nature of the constraint force screw, a set of constraint forces that are coplanar and parallel to each other can limit the rotation DOF in which the rotation axis is perpendicular to the plane where the constraint force screws are located. When the constraint force screws are coplanar and not parallel, the actuator has the rotation DOF. In conclusion, the number of constraint force screws only needs to be one set and, when the number increases, it will not have other effects on the actuator.

Therefore, while constructing the limb constrained triangle, it is necessary to make the modified actuator have the same kinematic properties as the original actuator as much as possible, which can be called the flexibility of limb constrained triangle. Reflected in the two types of limb kinematic chains is the ratio of the motion trajectory of j_{i2} with constraint to the trajectory of j_{i2} without constraint.

The motion trajectories of j_{i2} in two limb kinematic chains are shown in Figure 9. The joint j_{i2} of the RRR limb kinematic chain rotates π radians around the X-axis with $l_{j_{i1}j_{i2}}$ as the radius without the constraint of limb constrained triangle. The motion trajectory of the center point of the joint j_{i2} is shown by the blue line in Figure 9a. Under the constraint of the limb constrained triangle, the motion of the center point of the j_{i2} joint is restricted because of the condition that $l_{j_{i1}j_{i2}} + l_{j_{i2}j_{i4}} > l_{j_{i1}j_{i4}}$ must be satisfied, and its motion trajectory is shown by the red line in Figure 9a. In the RPR limb kinematic chain, the length of $l_{j_{i1}j_{i2}}$ needs to satisfy the condition that $0 < l_{j_{i1}j_{i2}} < 3500$, and the motion trajectory of the joint center point of $l_{j_{i1}j_{i2}}$ under this constraint condition is shown by the red line in Figure 9b. When there is no constraint, the joint center point of $l_{j_{i1}j_{i2}}$ can rotate π radians around the X-axis with $l_{j_{i1}j_{i2}}$ as the radius, and the motion trajectory is shown by the blue line in Figure 9b (in order to make the comparison between two motion trajectories clear, the unconstrained motion trajectories are sparsely processed).

(**a**)　　　　　　　　　　　　　　　　　　　　　　　(**b**)
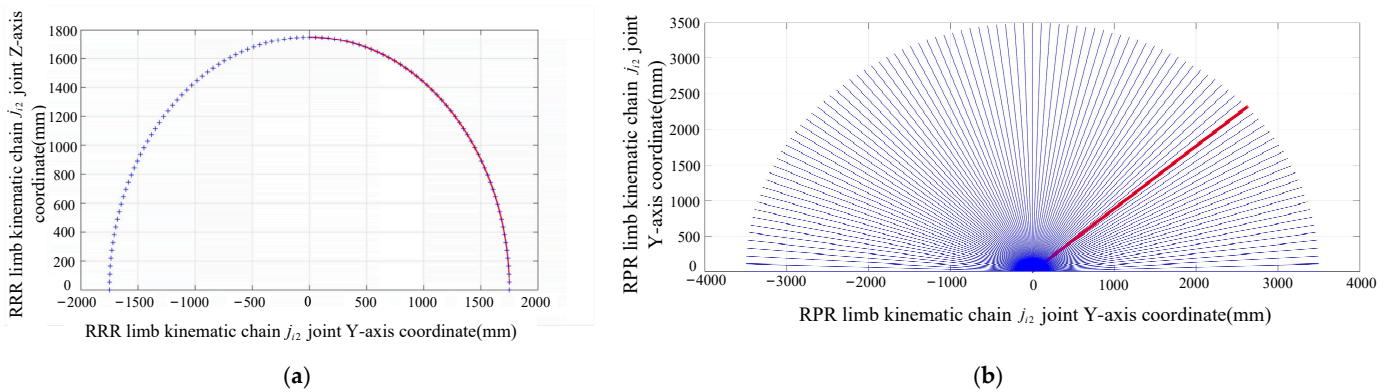
Figure 9. j_{i2} of the RRR and RPR limb kinematic chain: (**a**) j_{i2} of the RRR limb kinematic chain; (**b**) j_{i2} of the RPR limb kinematic chain.

When solving the trajectory of the center point of the j_{i2} joint in the RRR limb kinematic chain, the length of $l_{j_{i1}j_{i2}}$ is set to $0 < l_{j_{i1}j_{i2}} < 3500$, and the increment from the minimum value to the maximum value is 1. When $l_{j_{i1}j_{i2}} = 1$, $\cos l_{j_{i1}j_{i2}} l_{j_{i1}j_{i4}} = 1/3500$, the angle $\angle l_{j_{i1}j_{i4}} l_{j_{i1}j_{i2}\,\text{max}}$ is about 1.5705 radians. When $l_{j_{i1}j_{i2}} = 3499$, $\cos l_{j_{i1}j_{i2}} l_{j_{i1}j_{i4}} = 3499^2/(2 \times 3499 \times 1750)$, the angle $\angle l_{j_{i1}j_{i4}} l_{j_{i1}j_{i2}\,\text{min}}$ is about 0.0239 radians. Compared with the unconstrained case, the angle between $l_{j_{i1}j_{i2}}$ and $l_{j_{i1}j_{i4}}$ varies from 0 to π radians. Therefore, the flexibility of the limb constrained triangle of the RRR limb kinematic chain is as follows:

$$\frac{\angle l_{j_{i1}j_{i4}} l_{j_{i1}j_{i2}\,\text{max}} - \angle l_{j_{i1}j_{i4}} l_{j_{i1}j_{i2}\,\text{min}}}{\pi} = \frac{1.5705 - 0.0239}{\pi} = 0.4923$$

Since the motion modes of the RPR limb kinematic chain and the RRR limb kinematic chain are different, the methods used to calculate the flexibility of the constrained triangle are also different. In the process of increasing the length of $l_{j_{i1}j_{i2}}$ from 0 to 3500, each length corresponds to a semicircular workspace with that length as the radius. In order to quantify the workspace, the process of increasing $l_{j_{i1}j_{i2}}$ from 0 to 3500 is divided into n_1 equal parts, and the process of increasing the angle between $l_{j_{i1}j_{i2}}$ and $l_{j_{i1}j_{i4}}$ from 0 to π is divided into n_2 equal parts. Therefore, the flexibility of limb constrained triangle of the RPR limb kinematic chain is calculated as follows:

$$\frac{n_1}{n_1 n_2} = \frac{1}{n_2} \tag{10}$$

Comparing the flexibility of limb constrained triangle of the RRR limb kinematic chain with the RPR limb kinematic chain, it can be obtained that when $n_2 = 1$ or $n_2 = 2$, the flexibility of the RPR limb constrained triangle is greater than that of the RRR limb constrained triangle. However, according to the length of the three sides of the RPR limb constrained triangle, the angle between $l_{j_{i1}j_{i2}}$ and $l_{j_{i1}j_{i4}}$ cannot reach 0.5π and π, and when

$n_2 = 1$ or $n_2 = 2$, the continuity of the motion of the RPR limb kinematic chain is worse than that of the RRR limb kinematic chain, resulting in poor operational stability of the actuator.

In conclusion, under the constraint of the limb constrained triangle, the flexibility of the RRR limb kinematic chain is better than that of the RPR limb kinematic chain, and the stability is better.

3.2. Comparison Analysis of Parallel Actuators Based on the Dynamics

The dynamic characteristics of two types of parallel actuators are compared and analyzed using the ADAMS software. In two virtual prototypes, the variation ranges of $l_{j_{i1}j_{i2}}$, $l_{j_{i1}j_{i4}}$ and $l_{j_{i2}j_{i4}}$ are as described in Section 3.1. Combined with Figures 5 and 8, the lengths of other components and the initial state of two actuators are given, as shown in Table 4.

Table 4. Simulation parameters (mm).

	2-RRR Limb Parallel Actuator			2-RPR Limb Parallel Actuator	
$l_{j_{i2}j_{i3}}$	$l_{x_{i2}X}$	$l_{j_{i1}j_{i4}}$	$l_{j_{i1}X}$	$l_{j_{i1}j_{i2}}$
1750	2000	Initial length: 1750	2000	Initial length: 1750

In the two types of limb parallel actuators, the length change of the $l_{j_{i1}j_{i2}}$ rod is used as the driving input of the actuator. When the mobile platforms of the 2-RRR parallel actuator and the 2-RPR parallel actuator move along the Z-axis, the driving input signal is $500\sin(0.05\pi \times time)$; when the mobile platform of the two parallel actuators rotate around the X-axis, the driving input signals are $500\sin(0.01\pi \times time)$ and $500\sin(0.05\pi \times time)$, respectively. The displacement and acceleration of the mobile platform along the Z-axis and the displacement and acceleration along the Y-axis are shown in Figures 10 and 11, respectively, when the mobile platforms of the two parallel actuators move and rotate.

(**a**)

(**b**)
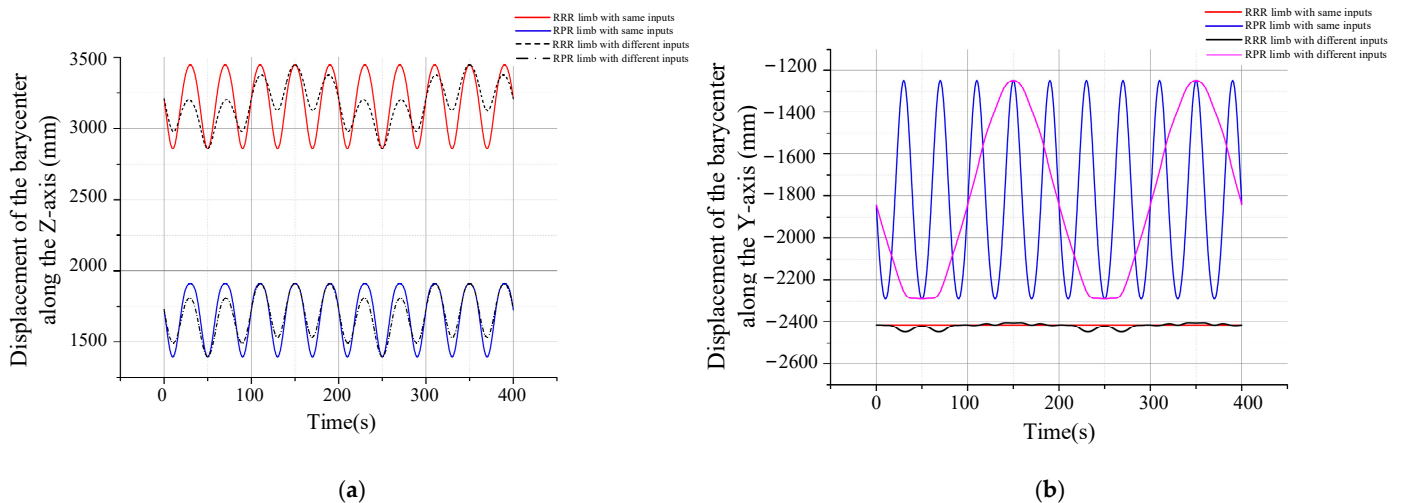
Figure 10. Displacement along Y-axis and Z-axis while lifting and rotating the RRR and RPR parallel platforms: (**a**) Displacement along Z-axis while lifting and rotating the RRR and RPR parallel platforms; (**b**) Displacement along Y-axis while lifting and rotating the RRR and RPR parallel platforms.

It can be seen from Figures 10 and 11 that when the input signals of two types of parallel actuators are the same, the stability of the 2-RRR parallel actuator in the Z-axis direction and the Y-axis direction are better than that of the 2-RPR parallel actuator. When the input signals of two types of parallel actuators are different, the displacement change of the 2-RRR parallel actuator mobile platform in the Y-axis direction is much smaller than that of the 2-RPR parallel actuator mobile platform. Compared with the acceleration

changes in the *Y*-axis and *Z*-axis directions, the stability of the 2-RRR parallel actuator is also better than that of the 2-RPR parallel actuator.

(**a**)   (**b**)
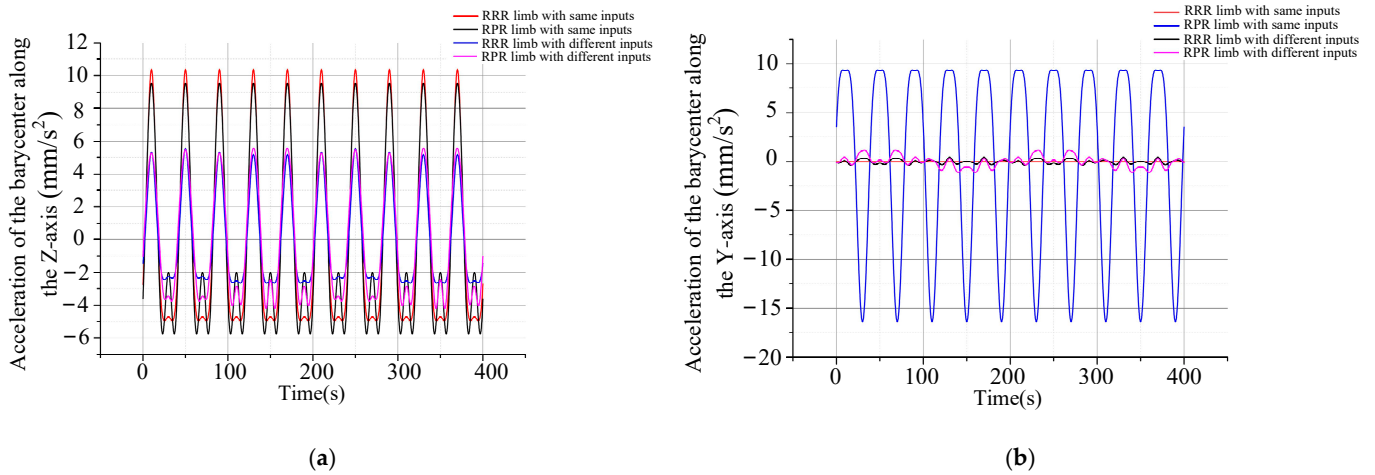
Figure 11. Acceleration along *Y*-axis and *Z*-axis while lifting and rotating the RRR and RPR parallel platforms: (**a**) Acceleration along *Z*-axis while lifting and rotating the RRR and RPR parallel platforms; (**b**) Acceleration along *Y*-axis while lifting and rotating the RRR and RPR parallel platforms.

According to the above analysis, under the constraint of the limb constrained triangle, the kinematic flexibility of the RRR limb kinematic chain is better than that of the RPR limb kinematic chain. Meanwhile, the 2-RRR parallel actuator is superior to the 2-RPR parallel actuator in terms of the position change of the barycenter of the mobile platform and the acceleration change of the barycenter with the same dimensions and the same input signal. Therefore, compared with the 2-RPR parallel actuator, the 2-RRR parallel actuator is more suitable for the vehicle lifting work of the stereo parking robot.

3.3. Selection of the Driving Link Based on the Failure Probability

Based on the determination that the 2-RRR parallel actuator is more suitable for the application of stereo parking robot, the selection of the driving links is carried out according to the structural characteristics of the 2-RRR parallel actuator.

As shown in Figure 12a, the triangle consisting of rod_1, rod_2, and $length_3$ provides a constrained triangle for the 2-RRR parallel actuator. Among them, rod_1 and rod_2 are rigid rods, and $length_3$ is a virtual connecting rod with length generated by the combination of motions of each kinematic pair. When considering the safety of the 2-RRR parallel actuator, the failure of the rigid rod can be controlled and the failure of the virtual connecting rod is uncontrollable. Therefore, the safety problems of the limb kinematic chain of 2-RRR parallel actuator are the failure of rod_1 and rod_2.

(**a**)   (**b**)
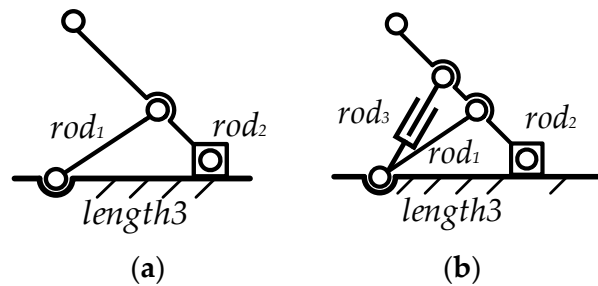
Figure 12. Original and modified limb kinematic chains of the 2-RRR parallel actuator: (**a**) Original limb kinematic chain; (**b**) Modified limb kinematic chain.

Taking normal and failure as the two states of the limb kinematic chain of 2-RRR parallel actuator, and P_{fail} is defined as the overall failure probability of the 2-RRR parallel

actuator. When the rod_1 fails alone, the 2-RRR parallel actuator is invalidated, and the probability of failure is $P_{fail1} = 0.5$; when the rod_2 fails alone, the 2-RRR parallel actuator is invalidated, and the probability of failure is $P_{fail2} = 0.5$; when the rod_1 and rod_2 fail at the same time, the 2-RRR parallel actuator is invalidated, and the probability of failure is $P_{fail3} = 0.5 \times 0.5 = 0.25$. The failure probability of the 2-RRR parallel actuator consists of P_{fail1}, P_{fail2}, and P_{fail3}.

In order to reduce each value without changing the kinematic properties of the 2-RRR parallel actuator, the limb kinematic chain of the 2-RRR parallel actuator is modified as shown in Figure 12b. Adding rod_3 as the driving rod, the DOF number of the 2-RRR parallel actuator is not changed. At this time, the failure probability P_{fail} of the 2-RRR parallel actuator is as follows: when rod_1 fails alone, the 2-RRR parallel actuator does not fail, and the probability of failure is $P_{fail4} = 0$; when rod_2 fails alone, the 2-RRR parallel actuator is invalidated, and the probability of failure is $P_{fail5} = 0.5$; when rod_3 fails alone, the 2-RRR parallel actuator does not fail, and the probability of failure is $P_{fail6} = 0$; when rod_1 and rod_3 fail at the same time, the 2-RRR parallel actuator is invalidated, and the probability of failure is $P_{fail7} = 0.5 \times 0.5 = 0.25$; when rod_1, rod_2, and rod_3 fail at the same time, the 2-RRR parallel actuator is invalidated, and the probability of failure is $P_{fail8} = 0.5 \times 0.5 \times 0.5 = 0.125$.

The failure probability of the 2-RRR parallel actuator composed of the modified limb kinematic chain consists of P_{fail4} to P_{fail8}. Compared with the failure probability of the 2-RRR parallel actuator before the modification, it can be found that the failure probability of the modified limb kinematic chain is smaller, except that rod_2 has the same failure probability under the failure condition. Meanwhile, it can be obtained from the P_{fail4} and P_{fail6} that rod_1 and rod_3 constitute a dual constrained triangle to ensure the security of the 2-RRR parallel actuator. In summary, it is safer to choose the limb kinematic chain as shown in Figure 12b.

3.4. Dimensional Optimization Based on Multi-Motion Performance Indexes

After determining the configuration of the 2-DOF parallel actuator, the overall structural parameters of the actuator need to be analyzed and researched to determine the optimal structural parameters of the actuator, and to provide the optimal motion transfer capability for the actuator, as well as to ensure the safety and stability. Based on the above studies, the sketch of a parallel lifting actuator is shown in Figure 13.
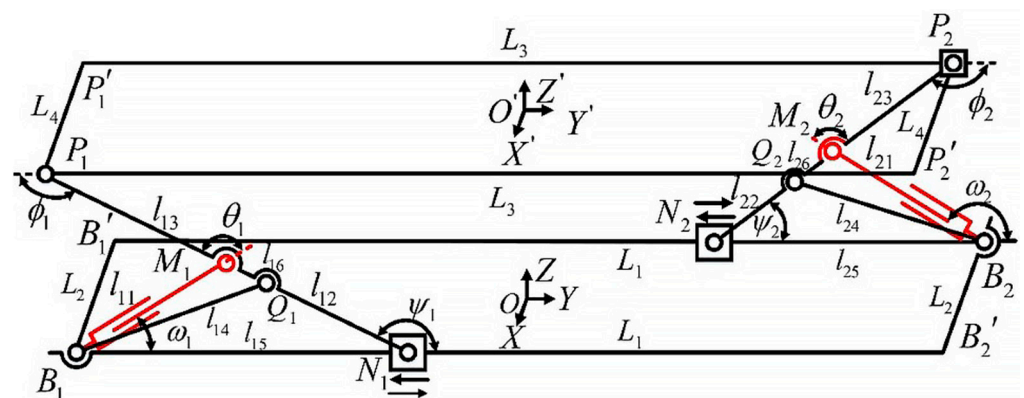
Figure 13. Sketch of a parallel lifting actuator on stereo parking robot.

In Figure 13, $B_1B_1'B_2B_2'$ is the fixed platform, $P_1P_1'P_2P_2'$ is the mobile platform, L_1 are the length of B_1B_2' and $B_1'B_2$, L_2 are the length of B_1B_1' and B_2B_2', L_3 are the length of P_1P_2' and $P_1'P_2$, and L_4 are the length of P_1P_1' and P_2P_2'. The origin of the overall coordinate system $O - XYZ$ is located at the center of the fixed platform, the X-axis direction is parallel to the B_1B_1' direction, the Y-axis direction is parallel to the B_1B_2' direction, and the Z-axis is perpendicular to the plane where the fixed platform is located. The origin

of the local coordinate system $O' - X'Y'Z'$ is located at the center of the mobile platform, the X'-axis direction is parallel to the P_1P_1' direction, the Y'-axis direction is parallel to the P_1P_2' direction, and the Z'-axis is perpendicular to the plane where the mobile platform is located. The length of the drive rod B_iM_i ($i = 1, 2$) in the parallel actuator is l_{i1}. The length between point Q_i and slider N_i is l_{i2}. The length between point M_i and point P_i on the mobile platform is l_{i3}. The length of rod B_iQ_i is l_{i4}. The distance between the base B_i and the slider N_i is l_{i5}. The length between point Q_i and point N_i is l_{i6}.

According to the isotropy evaluation index, the singular degree evaluation index, and working space index proposed in the literature [18,19], the parameters of each component of the 2-DOF parallel actuator are finally determined as shown in Table 5. Under these parameters, the average value of the singular degree evaluation index and the isotropy evaluation index are the lowest, and the isotropy evaluation index shows that the actuator has great kinematic performance, thus, ensuring the overall stability of the actuator.

Table 5. Parameters of components of the parallel actuator.

Dimensions of Each Component (mm), *i* = 1,2				
l_{i1}	l_{i1}	l_{i1}	l_{i1}	l_{i1}
1200~1750	1750	1155	1750	595
Platform parameters				
Length of L_1		Length of L_2	Length of L_3	Length of L_4
4000		1500	4000	1500

4. Experimental Research on Parallel Lifting Actuator on Stereo Parking Robot

4.1. Verification Model System for Parallel Lifting Actuator on Stereo Parking Robot

The verification model system of the parallel lifting actuator on the stereo parking robot is shown in Figure 14.
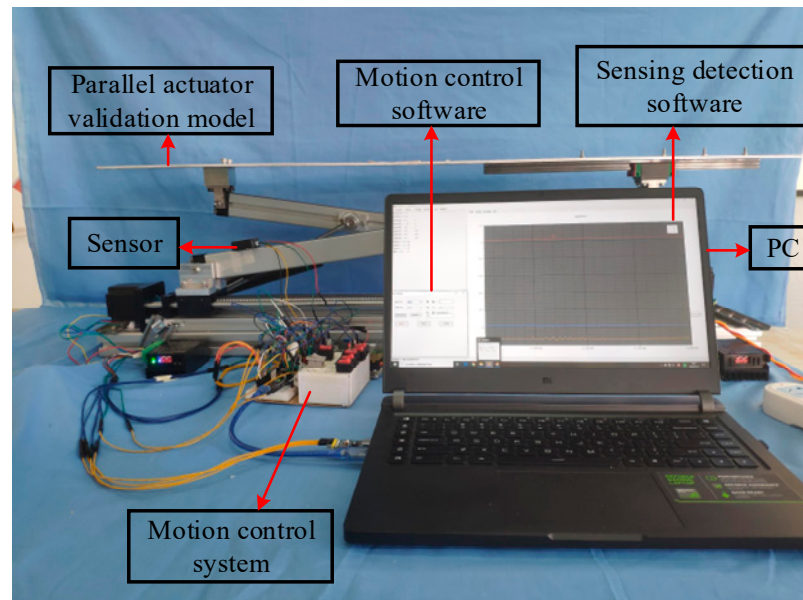
Figure 14. Verification model system of the parallel actuator on the stereo parking robot.

The system consists of a computer, a verification model, a motion control system, sensor detection software, motion control software, and sensors. The sensor is a 9-axis accelerometer sensor, which can measure the angle, angular velocity, and acceleration of the XYZ axes of the world coordinate system. The sampling interval is 0.1 s, and the

measurement errors are $0.01°$, $0.05°/s$, and 0.05 g, respectively. Considering the accuracy of the sensor and the machining error of the verification model, the sensor is not directly arranged at the barycenter of the mobile platform. Instead, the sensor is arranged on the N_iP_i rod of the verification model, and the acceleration along the Y-axis and Z-axis of the world coordinate system at the barycenter of the mobile platform is indirectly measured by measuring the angle and angular velocity of N_iP_i.

4.2. Verification Model of Parallel Lifting Actuator on Stereo Parking Robot

Figure 15 shows the verification model of the parallel actuator on a stereo parking robot. The verification model consists of a fixed platform, a mobile platform, a screw sliding table, and various connecting rods. The verification model uses B_iN_i as the driving link to facilitate the construction and control of the verification model.
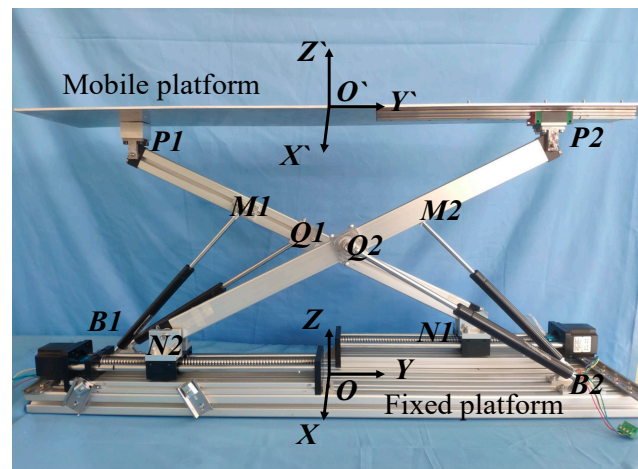
Figure 15. Verification model of a parallel lifting actuator on a stereo parking robot.

As shown in Figure 16, the different postures of the verification model are shown in (a–d), which are the initial posture, lifting posture, right rotation posture, and left rotation posture of the model, respectively. The correctness and effectiveness of the type synthesis theory of the parallel lifting actuator on a stereo parking robot can be concluded from Figures 15 and 16.

(a)   (b)   (c)   (d)

Figure 16. Different postures of the verification model: (**a**) Initial posture; (**b**) Lifting posture; (**c**) Right rotation posture; (**d**) Left rotation posture.

4.3. Verification of the Dynamic Characteristics of the Model Mobile Platform under Different Load Conditions

In this section, the dynamic characteristics tests of the model mobile platform under different load conditions were carried out. Different load tests with a drive speed of 12.5 mm/s were carried with loads of 500 g, 1000 g, and 1500 g, respectively. The acceleration value of the mobile platform of the verification model along the Y-axis and Z-axis is shown in Figure 17.
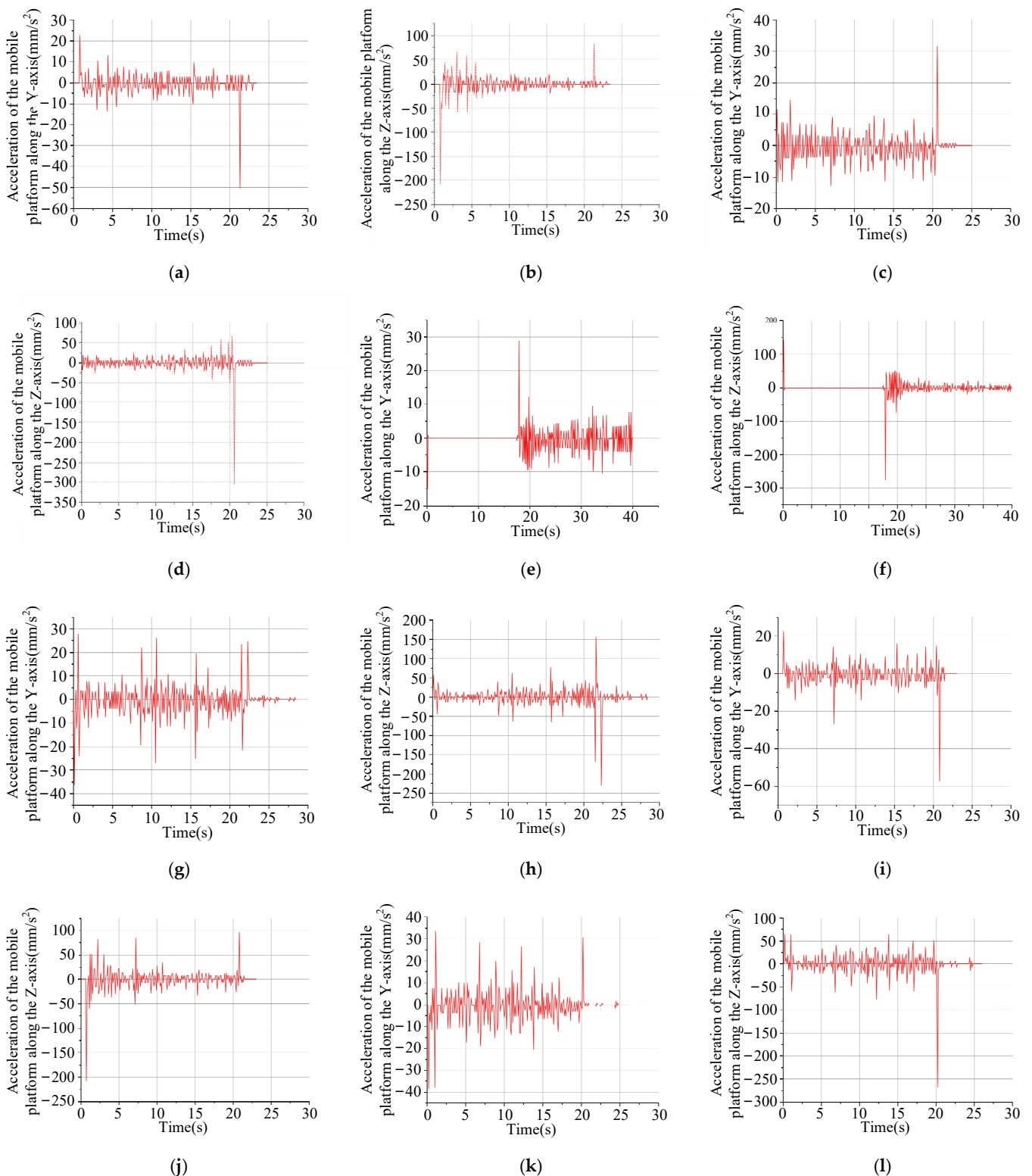
Figure 17. Dynamic characteristics of the mobile platform with a load of 500 g/1000 g/1500 g: (**a**) Rising process, load is 500 g; (**b**) Rising process, load is 500 g; (**c**) Falling process, load is 500 g; (**d**) Falling process, load is 500 g; (**e**) Rising process, load is 1000 g; (**f**) Rising process, load is 1000 g; (**g**) Falling process, load is 1000 g; (**h**) Falling process, load is 1000 g; (**i**) Rising process, load is 1500 g; (**j**) Rising process, load is 1500 g; (**k**) Falling process, load is 1500 g; (**l**) Falling process, load is 1500 g.

The mean value and standard deviation of the above data sets are shown in Table 6.

Table 6. Mean value and standard deviation of mobile platform's acceleration along the *Y*-axis and *Z*-axis with different loads.

	Mean Value/Standard Deviation		
	Load 500 g	Load 1000 g	Load 1500 g
Acceleration along the *Y*-axis when rising	2.92/3.94	3.07/4.03	3.70/4.91
Acceleration along the *Z*-axis when rising	9.04/14.31	9.70/14.79	11.06/15.69
Acceleration along the *Y*-axis when falling	3.33/4.53	3.85/5.15	4.53/6.14
Acceleration along the *Z*-axis when falling	9.56/13.29	11.39/15.14	13.36/18.00

According to Table 6, with the increase of loads, the mean value and standard deviation of the acceleration of the *Y*-axis and *Z*-axis directions are increasing in the rising and falling process, and the increasing range is getting larger. For example, the mean value/standard deviation of the *Y*-axis acceleration in the rising process is only 2.92/3.94 when the load is 500 g, but increases to 3.07/4.03 when the load is 1000 g and to 3.70/4.91 when the load is 1500 g. In addition, the mean value/standard deviation of acceleration in the falling process is larger than that in the rising process, due to the effect of gravitational acceleration. Taking the load as 1500 g as an example, the mean value/standard deviation of the *Y*-axis acceleration in the rising process is 3.70/4.91, and the mean value/standard deviation of the *Y*-axis acceleration in the falling process is 4.53/6.14. In summary, it can be concluded that, overall, the motion stability of the mobile platform of the verification model decreases with the increase of load mass in the presence of load, which provides a solid theoretical basis for improving the safety and stability of the actuator.

4.4. Practical Application Experiment of Parallel Lifting Actuator on Stereo Parking Robot

The Figure 18 shows the experimental environment of the parallel lifting actuator on the stereo parking robot.

Figure 18. Experimental environment of the parallel lifting actuator on the stereo parking robot.

The Figure 19 shows the lifting process of the stereo parking robot.

The stereo parking robot relies on its own moving system and lifting actuator to carry and access vehicles in the stereo garage with tracks. Figure 20a shows the robot moving system, Figure 20b shows the layout of the moving system, and Figure 20c is the plane sketch of the stereo garage.
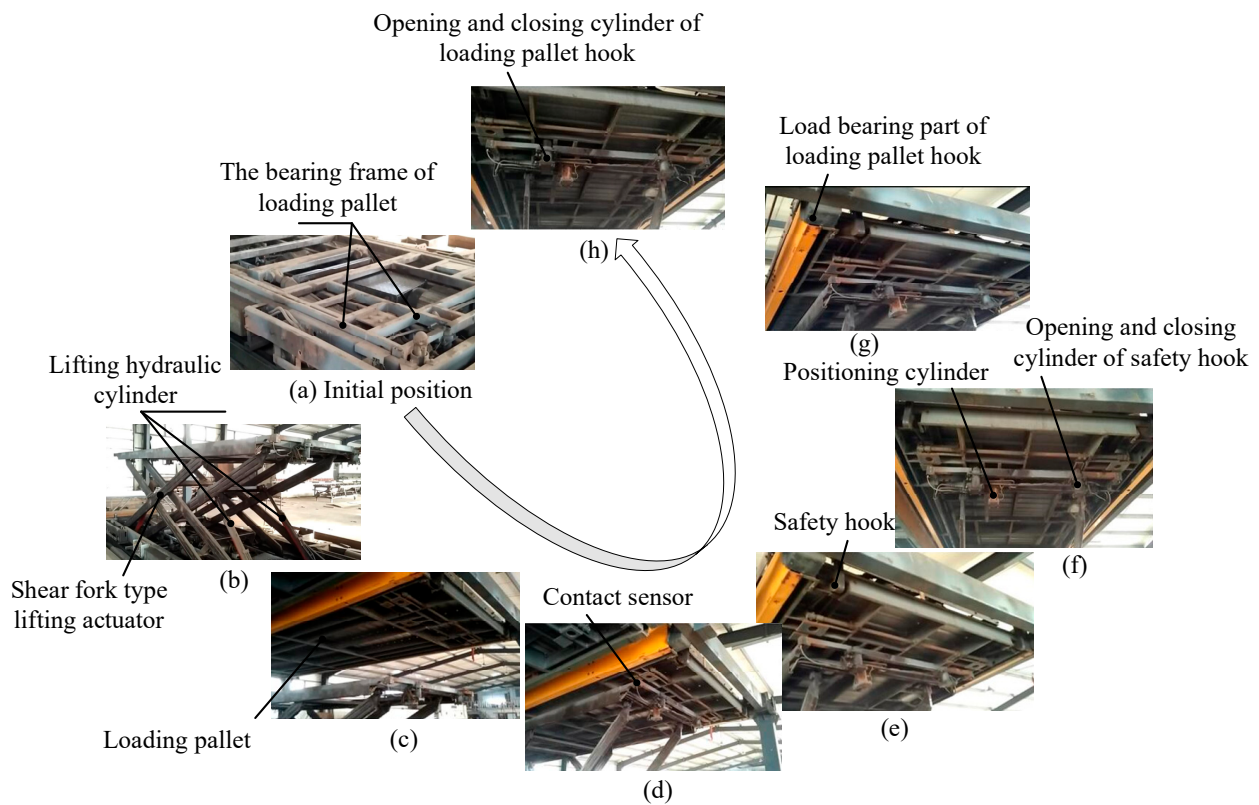
Figure 19. Lifting process of a stereo parking robot.

(**a**)   (**b**)   (**c**)
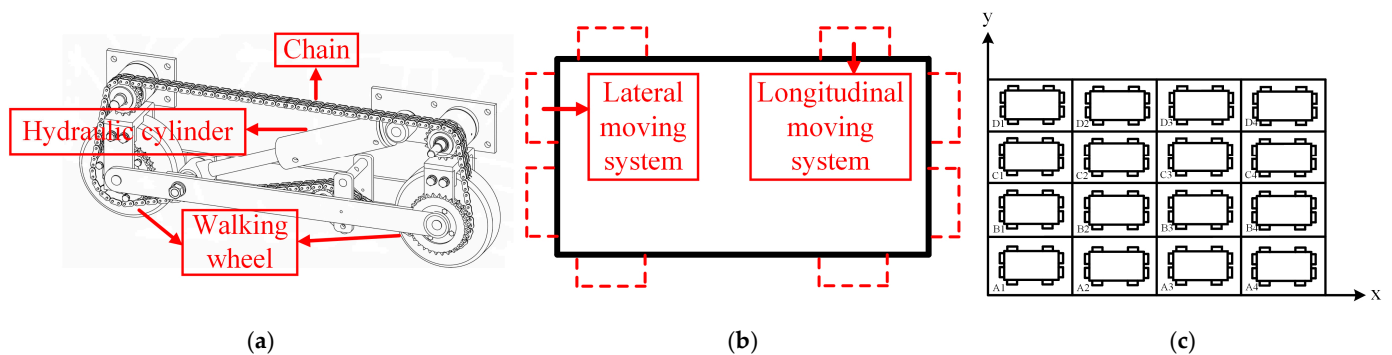
Figure 20. Moving system of the transporting system: (**a**) Moving system of the stereo parking robot; (**b**) Arrangement of the moving system on the stereo parking robot; (**c**) Plan sketch of the stereo garage.

The moving system can be contacted and separated from the track by the expansion and contraction of the hydraulic cylinder shown in Figure 20a. The lateral moving system and the longitudinal moving system are switched at the intersection, as shown in Figure 20c, to realize the all-round movement in the stereo garage. When combined with the lifting actuator, the all-round access of vehicles in the three-dimensional garage can be realized.

5. Conclusions

In this paper, in view of the safety and stability problems of the current stereo parking actuator, the parallel mechanism is used as the carrier to design and develop the parallel lifting actuator on the stereo parking robot, so as to improve the safety and stability of stereo parking equipment. Meanwhile, by converting the motion demand of the stereo parking robot into the DOF problem of the parallel actuator, the 2-DOF parallel mechanism (rotating around the *X*-axis and moving along the *Z*-axis of the overall coordinate system)

is determined as the main body of the parallel lifting actuator on the stereo parking robot. Based on the screw theory, a comprehensive study of the 2-DOF parallel actuator is carried out, and all constraint-4 screw systems corresponding to the 2-DOF parallel actuator are studied. On this basis, two limb kinematic chains are proposed to meet the requirements of the parallel lift actuator of the stereo garage robot. According to the proposed concept of a limb constrained triangle, the problem of no centroid during the operation of the 2-DOF parallel actuator is solved, and the movement DOF of the parallel lifting actuator along the *Y*-axis is constrained to obtain a parallel lifting actuator with one rotation DOF around the *X*-axis and one movement DOF along the *Z*-axis. According to the proposed concept of constrained triangle flexibility, a limb kinematic chain with a flexibility of 0.4923 is selected. The concept of failure probability is proposed by comparison, the minimum value of failure probability of the actuator is reduced from 0.25 to 0, the driving mode of the 2-DOF parallel actuator is determined, and the safety and stability of the 2-DOF parallel actuator are improved. Based on the isotropy evaluation index, singular degree evaluation index and working space index, the dimensional optimization of the actuator is completed, which further improves the safety and stability of the actuator. Finally, the validity of the actuator is proven by building a verification model system, and, by verifying the dynamic mechanical characteristics of the model mobile platform under different load conditions, it is proven that the kinematic stability of the verification model mobile platform decreases with the increase of the load mass under loaded condition, which provides a solid theoretical basis for improving the safety and stability of the actuator. Additionally, the 2-DOF parallel actuator is applied to a stereo parking robot, which can realize all-round movement and vehicle access in the stereo garage when arranged with tracks and structural frames, providing an effective solution to effectively alleviate the parking problem.

Author Contributions: Conceptualization, J.J., Q.T. and T.H.; methodology, software and writing—original draft preparation, T.H.; validation, visualization and writing—review and editing, Q.T.; formal analysis and investigation, J.S.; resources and data curation, J.Z. All authors have read and agreed to the published version of the manuscript.

Institutional Review Board Statement: Not applicable.

Informed Consent Statement: Not applicable.

Data Availability Statement: Not applicable.

Conflicts of Interest: The authors declare no conflict of interest.

References

1. Chen, X.J. National car ownership reached 281 million. *Automot. Obs.* **2021**, *1*, 7.
2. Wang, J.Q.; Zhan, Y.T.; Li, S.J. Analysis of the relationship between traffic congestion and the population density and car ownership of the surrounding communities. *Auto Time* **2020**, *9*, 32–33.
3. Li, Y.F.; Wang, Q.H. Talking about the development prospect and popularization and application of mechanical stereo parking garage. *Mod. Manuf. Technol. Equip.* **2019**, *8*, 105–106.
4. Zhang, W.S.; Zhao, J.; Ren, J. Stereo parking equipment industry overview and development trend analysis. *Intern. Combust. Engine Parts* **2021**, *11*, 210–211.
5. Song, Q.H.; Lu, J.N.; Wang, H.H. Design and simulation of push-pull driving mechanism for automatic parking spaces' pallets. *Appl. Mech. Mater.* **2014**, *488–489*, 1112–1116. [CrossRef]
6. Zheng, R.; Li, Y.H.; Lu, W.Z.; Wang, S.X.; Feng, Y.R.; Geng, X.Y. The Design and analysis of inclined stereo parking garage for old residential district reconstruction. *Mech. Eng. Technol.* **2019**, *8*, 315–326. [CrossRef]
7. Zhang, W.J.; Ye, R.Z.; Dong, F. Study of a new type of movable non-avoidance stereo parking device. In Proceedings of the 2020 IEEE International Conference on Artificial Intelligence and Computer Applications, Dalian, China, 27–29 June 2020; pp. 918–923.
8. Wang, Z.Y.; Li, X.; Su, X.H. Design of lifting mechanism of non avoiding side direction stereo parking equipment based on ADAMS. *Automob. Appl. Technol.* **2020**, *13*, 87–89.

9. Yan, J.Q.; Liu, C.Y.; Chen, S.Y.; Jiang, Z.H.; Ren, Z.J. Design of stereo parking device without avoidance based on multi-link. *Sci. Technol. Innov.* **2020**, *13*, 8–10.
10. Xia, Q.; Zhang, J.L. Structural design of two-position six-car parking device. *Technol. Innov. Appl.* **2019**, *32*, 91–92.
11. Ye, J.G.; Zhang, Y.J.; Lei, M.R.; Zheng, J. Design of double-deck auxiliary parking device on roadside. *Electron. Technol. Softw. Eng.* **2020**, *19*, 113–115.
12. Zheng, L.P.; Liang, Y.L.; Liu, H.C.; Meng, L.H. Multi-service station parking equipment for hydraulic clip lifting and reversing. *Mach. Des. Manuf.* **2021**, *7*, 250–254.
13. Wang, Y.H. Mechanical system research of simple three-dimensional parking equipment without avoidance. *Mod. Ind. Econ. Inf.* **2021**, *8*, 103–104.
14. Zhang, T.Y.; Qin, T.; Wu, K.; Jin, C.; Cao, Y.H.; Wang, W. Design of a Small column-type stereo parking device. *Mech. Res. Appl.* **2019**, *3*, 130–132.
15. Chen, Z.H.; Li, J.H.; Wang, S.K.; Wang, J.Z.; Ma, L.L. Flexible gait transition for six wheel-legged robot with unstructured terrains. *Robot. Auton. Syst.* **2022**, *150*, 103989. [CrossRef]
16. Wang, J.S.; Huang, T. Parallel machine tool-opportunities and challenges facing the machine tool industry. *China Mech. Eng.* **1999**, *10*, 31–35.
17. Huang, Z.; Zhao, Y.S.; Zhao, T.S. *Advanced Spatial Mechanism*, 2nd ed; Higher Education Press: Beijing, China, 2014.
18. Jiang, J.G.; Wu, D.H.; He, T.H.; Zhang, Y.D.; Li, C.P.; Sun, H. Kinematic analysis and energy saving optimization design of parallel lifting mechanism for stereoscopic parking robot. *Energy Rep.* **2022**, *8*, 2163–2178. [CrossRef]
19. He, T.H.; Shao, J.P.; Zhang, Y.D.; Jiang, J.G. Kinematic performance evaluation of 2-DOF parallel mechanism applied in multilayer garage. *Adv. Mech. Eng.* **2018**, *10*, 168781401879171. [CrossRef]